Bonding Analysis in Inorganic Transition-Metal Cubic Clusters. 3. Metal-Centered Tetracapped $M_9(\mu_5\text{-}E)_4L_n$ Species with a Tetragonal Distortion

Bachir Zouchoune,† François Ogliaro, Jean-François Halet,* and Jean-Yves Saillard*

Laboratoire de Chimie du Solide et Inorganique Moléculaire, UMR CNRS 6511, Université de Rennes 1, 35042 Rennes Cedex, France

Jeffrey R. Eveland and Kenton H. Whitmire*

Department of Chemistry, Rice University, Houston, Texas 77251

Received June 12, 1997

A number of main group element (E)−transition metal (M) cluster compunds based upon a hexacapped M_8 cube have been reported in two configurations: empty and with interstitial metal atoms in the center of the cube. Related molecules arise upon slow oxidation of the reaction product that forms when $[Bi_2Co_4(CO)_{11}]^-$ is treated with $Mo(CO)_3$(toluene) giving Bi−Co clusters based upon tetragonally distorted tetracapped cubic metal arrays with interstitial metal atoms. These compounds formulated as $[PPN]_2[Bi_4Co_9(CO)_{16}]\cdot 2THF$ ($[PPN]_2[\mathbf{1}]\cdot 2THF$) and $[PPN]_2[Bi_8Co_{14}(CO)_{20}]\cdot 1.08THF$($[PPN]_2[\mathbf{2}]\cdot 1.08THF$) have been characterized via single-crystal X-ray diffraction. An alternative description ascribes the metal cores to close-packed arrays based upon the cuboctahedron. The complexes are electron rich via conventional electron-counting formalisms. To understand these molecules more fully, a thorough theoretical analysis of compounds $[\mathbf{1}]^{2-}$ and $[\mathbf{2}]^{2-}$ was undertaken. The calculations indicate that the bonding of the interstitial metal atom with the metallic host somewhat differs from that found in their related metal-centered cubic species $M_9(\mu_4\text{-}E)_6L_8$, due to stretching along the 4-fold axis. The HOMO−LUMO region is slightly antibonding between the Co_i atoms (i = interstitial) and the surrounding Bi and Co_p (p = peripheral) atoms. As with other members of this cubic cluster class, no HOMO−LUMO gaps are observed. The actual electron counts for $[\mathbf{1}]^{2-}$ and $[\mathbf{2}]^{2-}$, however, favor stronger Co_p-Co_i and $Bi-Co_i$ bonding than would be observed for the allowed higher electron counts. Crystallographic data for $[PPN]_2[\mathbf{1}]\cdot 2THF$: triclinic space group $P\bar{1}$; $a = 13.560(5)$, $b = 15.893(5)$, $c = 11.884(4)$ Å; $\alpha = 105.26(2)$, $\beta = 98.25(3)$, $\gamma = 83.25(3)°$; $Z = 1$. Crystallographic data for $[PPN]_2[\mathbf{2}]\cdot 1.08THF$: triclinic space group $P1$; $a = 17.445(5)$, $b = 18.234(3)$, $c = 9.033(3)$ Å; $\alpha = 92.74(2)$, $\beta = 102.59(3)$, $\gamma = 78.52(2)°$; $Z = 1$.

Introduction

In the past several years a number of compounds having cubic or distorted-cubic M_8 cluster geometries have been encountered in which some or all of the faces are capped by main group element fragments. These cubic arrays may be empty[1−11] or centered by an interstitial atom.[12−17] The electronic structures of empty $M_8(\mu_4\text{-}E)_6L_8$ clusters and metal-centered $M_9(\mu_4\text{-}E)_6L_8$ were discussed.[18,19] This hexacapped cubic (HCC) system is interesting in the variability of the electron counts that are observed for the different cluster compounds. Theory predicts the existence of certain magic numbers (120 MVEs for the

† Permanent address: Institut de Chimie, Département de Chimie Inorganique, Université de Constantine, Constantine, Route de Aïn-el-Bey, Algeria.

(1) Lower, L. D.; Dahl, L. F. *J. Am. Chem. Soc.* **1976**, *98*, 5046.
(2) Fenske, D.; Basoglu, R.; Hachgenei, J.; Rogel, F. *Angew. Chem., Int. Ed. Engl.* **1984**, *23*, 160.
(3) Fenske, D.; Magull, J. *Z. Naturforsch.* 1990, *45b*, 121.
(4) Fenske, D.; Krautscheid, H.; Müller, M. *Angew. Chem., Int. Ed. Engl.* **1992**, *31*, 321.
(5) Fenske, D.; Hachgenei, J.; Ohmer, J. *Angew. Chem., Int. Ed. Engl.* **1985**, *24*, 706.
(6) Fenske, D.; Ohmer, J.; Hachgenei, J.; Merzweiler, K. *Angew. Chem., Int. Ed. Engl.* **1988**, *27*, 1277.
(7) Fenske, D.; Hachgenei, J.; Rogel, F. *Angew. Chem., Int. Ed. Engl.* **1984**, *23*, 982.
(8) Christou, G.; Hagen, K. S.; Bashkin, J. K.; Holm, R. H. *Inorg. Chem.* **1985**, *24*, 1010.
(9) (a) Pohl, S.; Opitz, U. *Angew. Chem., Int. Ed. Engl.* **1993**, *32*, 863. (b) Pohl, S.; Barklage, W.; Saak, W.; Opitz, U. *J. Chem. Soc., Chem. Commun.* **1993**, 1251.
(10) Junghans, C.; Saak, W.; Pohl, S. *J. Chem. Soc., Chem. Commun.* **1994**, 2327.
(11) Pohl, S.; Saak, W. *Angew. Chem., Int. Ed. Engl.* **1984**, *23*, 907.
(12) Zebrowski, J. P.; Hayashi, R. K.; Bjarnason, A.; Dahl, L. F. *J. Am. Chem. Soc.* **1992**, *114*, 3121.
(13) Fenske, D.; Persau, C. *Z. Anorg. Allg. Chem.* **1991**, *593*, 61.
(14) Fenske, D.; Ohmer, J.; Merzweiler, K. *Angew. Chem., Int. Ed. Engl.* **1988**, *27*, 1512.
(15) Brennan, J. G.; Siegrist, T.; Stuczynski, S. M.; Steigerwald, M. L. *J. Am. Chem. Soc.* **1989**, *111*, 9240.
(16) Fenske, D.; Fleischer, H.; Persau, C. *Angew. Chem., Int. Ed. Engl.* **1989**, *28*, 1665.
(17) (a) Fenske, D.; Vogt, K. Unpublished results. (b) Vogt, K. Ph.D. Dissertation, University of Karlsruhe, Germany, 1994.
(18) (a) Furet, E.; Le Beuze, A.; Halet, J.-F.; Saillard, J.-Y. *J. Am. Chem. Soc.* **1994**, *116*, 274. (b) Furet, E.; Le Beuze, A.; Halet, J.-F.; Saillard, J.-Y. *J. Am. Chem. Soc.* **1995**, *117*, 4936.
(19) (a) Rösch, N.; Ackermann, L.; Pacchioni, G. *Inorg. Chem.* **1993**, *32*, 2963. (b) Hoffman, G. G.; Bashkin, J. K.; Karplus, M. *J. Am. Chem. Soc.* **1990**, *112*, 8705. (c) Lauher, J. W. *J. Am. Chem. Soc.* **1978**, *100*, 5305. (d) Burdett, J. K.; Miller, G. J. *J. Am. Chem. Soc.* **1987**, *109*, 4081 (e) Wheeler, R. A. *J. Am. Chem. Soc.* **1990**, *112*, 8737. (f) Nomikou, Z.; Schubert, B.; Hoffmann, R.; Steigerwald, M. L. *Inorg. Chem.* **1992**, *31*, 2201.

S0020-1669(97)00715-5 CCC: $15.00
Published on Web 02/12/1998

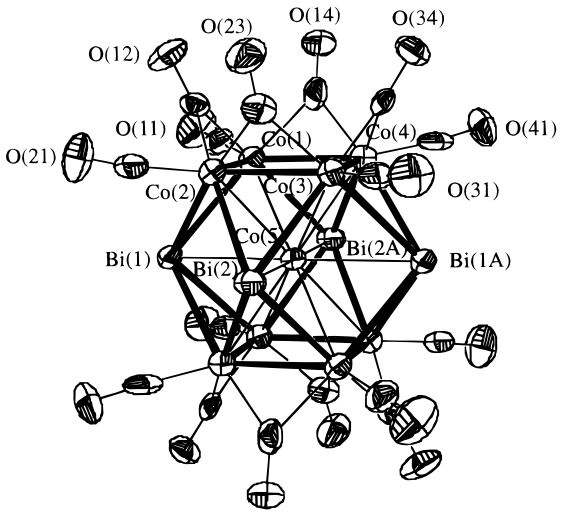

Figure 1. Thermal ellipsoid plot of the anionic portion of $[PPN]_2[\mathbf{1}]\cdot 2THF$, showing 50% probability thermal ellipsoids and the atom-labeling scheme.

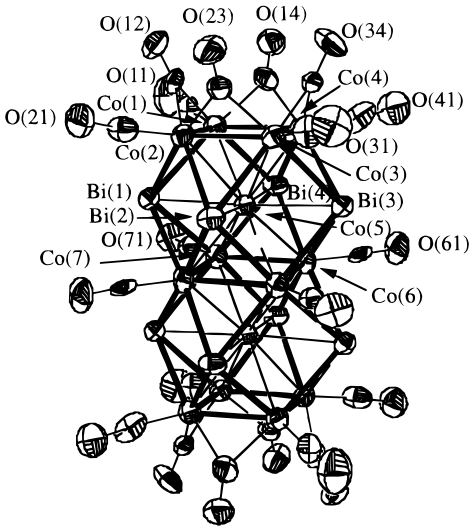

Figure 2. Thermal ellipsoid plot of the anionic portion of $[PPN]_2[\mathbf{2}]\cdot 1.08THF$, showing 50% probability thermal ellipsoids and the atom-labeling scheme.

empty compounds; 124 MVEs for the metal-centered species; MVE = metal valence electron) but allows for a range of electron counts. Values ranging from 99 to 120 MVEs for the empty and 120 to 130 MVEs for the centered clusters have been reported so far. Recently we published a preliminary report of the synthesis and structural characterization of $[PPN]_2[Bi_4Co_9(CO)_8(\mu\text{-}CO)_8]$ ($[PPN]_2[\mathbf{1}]$) and $[PPN]_2[Bi_8Co_{14}(CO)_{12}(\mu\text{-}CO)_8]$ ($[PPN]_2[\mathbf{2}]$), which are derived from centered cubic arrays but for which only four of the faces are capped.[20] These tetracapped cubic (TCC) compounds are of interest because they expand the reported range of electron counts and structural types for cubic species. In this paper we present the full structural details of $[PPN]_2[\mathbf{1}]\cdot 2THF$ (Figure 1) and $[PPN]_2[\mathbf{2}]\cdot 1.08THF$ (Figure 2) along with extended Hückel (EH) and density functional theory (DFT) calculations undertaken to understand the unusual bonding situation.

These clusters were encountered as products of the oxidation of the intermediate that arose when the anionic $[Bi_2Co_4(CO)_{11}]^{-/2-}$ (**7**) (see Chart 1) were treated with $Mo(CO)_3$(toluene). The

Chart 1

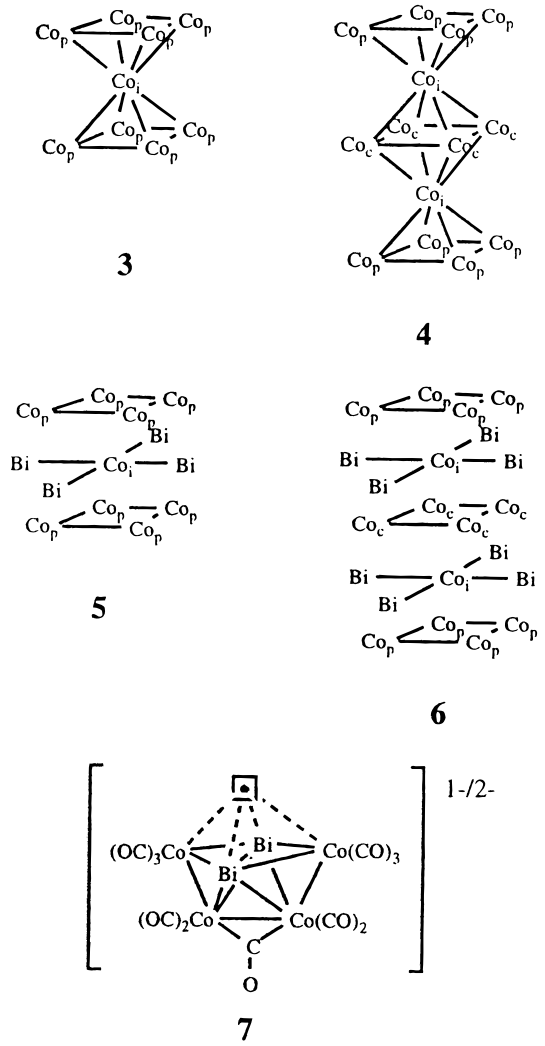

metal cores of the anions **7** may be viewed as either a *nido*-pentagonal bipyramid or an *arachno*-dodecahedron.[23] Either view, however, does not predict the observed Bi−Bi bonding interaction. A bonding analysis of **7** has shown that this formally electron-rich core structure's high electron count is due to a mismatch in the orbitals of Bi versus Co leading to nonbonding orbitals which can accommodate the extra electrons. When we examined the chemistry of this unusual molecule, it occurred to us that there was a possibility that the "missing" vertex in the *nido*-pentagonal bipyramidal structure may be filled by a suitable metal fragment. We were particularly interested in discovering if the Bi−Bi interaction would persist in such a structure. The reagent $Mo(CO)_3$(toluene) was chosen to supply a $Mo(CO)_3$ fragment as that group should add no additional electrons to the cluster electron count. While the anticipated structure would have been interesting given the rarity of pentagonal bipyramidal clusters, the higher nuclearity species proved to be even more intriguing both from a structural and from a bonding perspective.

Experimental Section

General Considerations. All reactions were performed using standard Schlenk techniques with an atmosphere of dry, oxygen-free

(20) Whitmire, K. H.; Eveland, J. R. *J. Chem. Soc., Chem. Commun.* **1994**, 1335.
(21) Whitmire, K. H.; Leigh, J. S.; Gross, M. E. *J. Chem. Soc., Chem. Commun.* **1987**, 926.
(22) Strohmeier, W. *Chem. Ber.* **1961**, *94*, 3337.
(23) Albright, T. A.; Yee, K. A.; Saillard, J.-Y.; Kahlal, S.; Halet, J.-F.; Leigh, J. S.; Whitmire, K. H. *Inorg. Chem.* **1991**, *30*, 1179.

nitrogen. Solvents were distilled from appropriate drying agents prior to use: MeOH (Mg); hexanes ($LiAlH_4$); THF and Et_2O ($LiAlH_4$ followed by Na/Ph_2CO). $BiCo_3(CO)_9$[21] and $Mo(CO)_3$(toluene)[22] were prepared by the literature methods, and $K[Bi_2Co_4(CO)_{11}]$ was prepared via a modification of the literature procedure,[23] in which KC_8 was employed as the reductant in place of Cp_2Co. KC_8 was prepared by slow addition of potassium metal to graphite heated to 190 °C under argon. Infrared spectra were measured on a Perkin-Elmer model 1640 FTIR spectrophotometer using 0.1 mm path length CaF_2 cells for solution and anhydrous potassium bromide pellets for solid-state spectra. ^1H and ^{13}C NMR spectra were obtained on a Bruker AC 250 spectrometer in the solvent noted. Magnetic data were obtained on a Quantum Design MPMS-5S SQUID magnetometer. Carbon monoxide analyses were performed on a high-vacuum line as previously described.[24]

Preparation of [PPN]$_2$[1]·2THF and [PPN]$_2$[2]·1.08THF. $BiCo_3(CO)_9$, 3.00 g (4.7 mmol), and KC_8, 0.70 g (5.2 mmol), were weighed into a flask under nitrogen and dissolved in 70 mL of THF. The resulting solution was stirred until all of the starting cluster was consumed, as measured by infrared spectroscopy, after which time it was filtered through fritted glass and $Mo(CO)_3$(toluene), 1.02 g (3.8 mmol), dissolved in THF was added to the filtrate. The resulting solution was allowed to stir for approximately 1 week until all of the $[Bi_2Co_4(CO)_{11}]^-$ was consumed. The solvent was removed in vacuo and the residue dissolved in MeOH. [PPN]Cl, 3.16 g (5.5 mmol), was introduced into the flask and the resulting mixture stirred for 1 h. The solvent was again removed under vacuum and the solid washed with several portions each of hexanes, Et_2O, and MeOH. The remaining solid was dried thoroughly under vacuum. This solid dissolves in THF to give the following IR spectrum (cm^{-1}): 1980 vs, 1940 s, 1891 m, 1779 w, 1726 w. The ^{13}C NMR spectrum taken in acetone-d_6 showed broad bands at 255.8 and 247.8 ppm along with bands assignable to the PPN^+ counterion at 134.7 s, 131.9 dd (^1J = 179 Hz), 131.9 dt (^1J = 179 Hz), and 128.4 dd (^1J = 107 Hz). This intermediate was found to be paramagnetic. The solid (1.00 g) was weighed into a flask under an atmosphere of nitrogen and then dissolved in approximately 50 mL THF and allowed to stand. Upon standing for ca. 1 month, needlelike crystals of [PPN]$_2$[**2**]·1.08THF grew. During attempts to repeat the reaction, it was discovered that slow introduction of air was necessary. If air is rigorously excluded, no reaction to form [PPN]$_2$[**1**] or [PPN]$_2$[**2**] was observed. When the air is introduced at a more rapid rate into these same solutions a mixture of block-shaped crystals of [PPN]$_2$[**1**]·2THF and crystals of [PPN]$_2$[**2**]·1.08THF was produced. For these experiments the solution was placed in a vacuum flask, and oxygen was introduced slowly in very small portions over several weeks on a vacuum line. Crystals of [PPN]$_2$[**1**]·2THF and [PPN]$_2$[**2**]·1.08THF grow at the solvent/atmosphere interface and settle slowly as their size increases. When a mixture is produced, crystals of the two compounds must be separated manually. The magnetic moment for [PPN]$_2$[**1**]·2THF was found to be 2.24 μ_B. IR (KBr, cm^{-1}): 1972 vs, br, 1890 m, 1837 mw.

X-ray Crystallographic Characterization of [PPN]$_2$[1]·2THF and [PPN]$_2$[2]·1.08THF. Structural data were collected on a fully automated Rigaku AFC5S single-crystal X-ray diffractometer using graphite-monochromated Mo Kα radiation (λ = 0.7107 Å). Data were corrected for Lorentz/polarization effects and absorption (ψ scans), but no decay correction was necessary for either crystal. Data collection and refinement parameters are given in Table 1. Both compounds crystallize in the triclinic crystal system with centrosymmetric space group $P\bar{1}$ chosen on the basis of the relative occurrence and intensity statistics, which was confirmed in both cases by successful structure solution and refinement. All non-hydrogen atoms in the anions and the P and N atoms of the cations were refined anisotropically. The carbon atoms of the cations were refined isotropically. Hydrogen atoms were included in their calculated positions via a riding model in which they were tied to the atom to which they are associated with fixed isotropic displacement parameters. Selected bond distances and angles for [PPN]$_2$[**1**]·2THF and [PPN]$_2$[**2**]·1.08THF are given in Tables 2 and 3. Full data collection and refinement parameters, atomic positions, bond distances and angles, anisotropic displacement parameters, and hydrogen atom coordinates are given in the Supporting Information.

Table 1. Crystallographic Data Collection and Refinement Parameters for [PPN]$_2$[**1**]·2THF and [PPN]$_2$[**2**]·1.08THF

	[PPN]$_2$[**1**]·2THF	[PPN]$_2$[**2**]·1.08THF
empirical formula	$C_{96}H_{76}Bi_4Co_9N_2O_{18}P_4$	$C_{96.32}H_{68.64}Bi_8Co_{14}N_2O_{21.08}P_4$
fw	3035.87	4212.18
temp (K)	223(2)	223(2)
cryst system (space group)	triclinic ($P\bar{1}$ (No. 2))	triclinic ($P\bar{1}$ (No. 2))
a (Å)	13.560(5)	17.445(5)
b (Å)	15.893(5)	18.234(3)
c (Å)	11.884(4)	9.033(3)
α (deg)	105.26(2)	92.74(2)
β (deg)	98.25(3)	102.59(3)
γ (deg)	83.25(3)	78.52(2)
V (Å^3)	2437(1)	2748(1)
Z	1	1
λ(Mo Kα) (Å)	0.7107	0.7107
ρ_{calc} (g/cm^3)	2.0686	2.5449
μ (cm^{-1})	87.882	148.84
final R indices		
R_1[a]	0.0328	0.0373
wR_2[a]	0.0348	0.0414

[a] $R_1 = \sum||F_o| - |F_c||/|F_o|$; w$R_2 = \{\sum[w(F_o^2 - F_c^2)^2]/\sum wF_o^4]\}^{1/2}$; $w^{-1} = [\sigma^2(F_o^2) + (aP^2) + bP]$; $P = [(F_o^2) + 2(F_c^2)]/3$.

Computational Details. (a) Geometry Idealization. The different molecular models used were based on the averaged idealized (D_{4h}) experimental molecular compounds. The following bond distances (Å) were used in the TTC cubic models: Co_p-Co_p = 2.47; Co_p-Co_i = 2.64; Co_p-Bi = 2.76; $Co_p-C(O)$ = 1.75; $Co_p-(\mu\text{-}C(O))$ = 1.91; C−O = 1.15; (μ-C)−O = 1.17 (subscript p denotes peripheral cobalt atoms and i the interstitial cobalt atom).

(b) Extended Hückel Calculations. Calculations have been carried out within the extended Hückel formalism[25] using the weighted H_{ij} formula[26] with the program CACAO.[27] The exponents (ζ) and the valence shell ionization potentials (H_{ii} in eV) were (respectively): 1.625, −21.4 for C 2s; 1.625, −11.4 for C 2p; 2.275, −32.3 for O 2s; 2.275, −14.8 for O 2p; 2.653, −15.75 for Bi 6s; 2.092, −10.52 for Bi 6p; 2.0, −9.21 for Co 4s; 2.0, −5.29 for Co 4p; 2.078. The H_{ii} value for Co 3d was set equal to −13.18. A linear combination of two Slater-type orbitals of exponents ζ_1 = 5.55 and ζ_2 = 1.9 with the weighting coefficients c_1 = 0.5551 and c_2 = 0.6461 was used to represent the Co 3d atomic orbitals.

(c) Density Functional Calculations. Single point calculations have been carried out on the anions of compounds $[\mathbf{1}]^{2-}$ and $[\mathbf{2}]^{2-}$ using the Amsterdam Density Functional (ADF) program[28] within the local density approximation (LDA).[29] The numerical integration procedure applied for the calculations was developed by te Velde et al.[30] The atom electronic configurations were described by a double-ζ Slater-type orbital (STO) basis set for C 2s and 2p and O 2s and 2p, a triple-ζ STO basis set for Bi 6s and 6p and Co 3d and 4s, and single-ζ STO function for Co 4p. A frozen-core approximation[31] was used to treat the core electrons of C, O, Co, and Bi.

Results

Synthesis of [PPN]$_2$[1] and [PPN]$_2$[2]. The compound $K[Bi_2Co_4(CO)_{11}]$ is obtained via reduction of $BiCo_3(CO)_9$ as

(24) (a) Hodali, H. Ph.D. Thesis, Northwestern University, 1979. (b) Bachman, R. E.; Miller, S. K.; Whitmire, K. H. *Organometallics* **1995**, *14*, 796.

(25) Hoffmann, R. *J. Chem. Phys.* **1963**, *39*, 1397.
(26) Ammeter, J. H.; Bürgi, H.-B.; Thibeault, J. C.; Hoffmann, R. *J. Am. Chem. Soc.* **1978**, *100*, 3686.
(27) Mealli, C.; Proserpio, D. M. *J. Chem. Educ.* **1990**, *67*, 399.
(28) (a) Baerends, E. J.; Ellis, D. E.; Ros, P. *Chem. Phys.* **1973**, *2*, 41. (b) Baerends, E. J.; et al. *Amsterdam Density Functional (ADF) program*, version 2.0.1; Vrije Universiteit: Amsterdam, Netherlands, 1996.
(29) Vosko, S. H.; Wilk, L.; Nusair, M. *Can. J. Phys.* **1980**, *58*, 1200.
(30) Boerrigter, P. M.; te Velde, G.; Baerends, E. J. *Int. J. Quantum Chem.* **1988**, *33*, 87.
(31) Baerends, E. J. Ph.D. Thesis, Vrije Universiteit, Amsterdam, Netherlands, 1975.

Table 2. Selected Bond Distances (Å) and Angles (deg) for $[PPN]_2[\mathbf{1}]\cdot 2THF$[a]

A. Distances

Bi(1*)−Co(1)	2.749(2)	Bi(1*)−Co(2)	2.745(2)
Bi(1)−Co(4)	2.722(2)	Bi(1)−Co(3)	2.729(2)
Bi(2)−Co(1)	2.735(2)	Bi(1)−Co(5)	2.709(1)
Bi(2*)−Co(3)	2.737(2)	Bi(2*)−Co(2)	2.757(2)
Bi(2)−Co(5)	2.7185(9)	Bi(2)−Co(4)	2.741(2)
Co(1)−Co(4)	2.480(2)	Co(1)−Co(2)	2.466(2)
Co(2)−Co(3)	2.461(2)	Co(1)−Co(5)	2.631(2)
Co(3)−Co(4)	2.470(2)	Co(2)−Co(5)	2.605(2)
Co(4)−Co(5)	2.607(2)	Co(3)−Co(5)	2.618(2)

B. Angles

Co(1*)−Bi(1)−Co(2*)	53.35(5)	Bi(2)−Co(1)−Co(2)	122.18(7)
Co(1*)−Bi(1)−Co(3)	90.09(6)	Bi(2)−Co(1)-Co(4)	63.20(6)
Co(1*)−Bi(1)−Co(4)	115.01(5)	Bi(2)−Co(1)-Co(5)	60.84(4)
Co(1*)−Bi(1)−Co(5)	57.64(4)	Co(2*)−Bi(1)−Co(4)	91.36(5)
Co(2*)−Bi(1)−Co(3)	114.58(5)	Co(2*)−Bi(1)−Co(5)	57.05(4)
Co(3)−Bi(1)−Co(4)	53.88(5)	Co(2)−Co(1)−Co(4)	88.28(7)
Co(3)−Bi(1)−Co(5)	57.55(4)	Co(2)−Co(1)−Co(5)	61.36(6)
Co(4)−Bi(1)−Co(5)	57.38(4)	Co(4)−Co(1)−Co(5)	61.26(6)
Co(1)−Bi(2)−Co(4)	53.85(5)	Co(3*)−Bi(2)−Co(4)	114.39(5)
Co(1)−Bi(2)−Co(5)	57.69(4)	Co(3*)−Bi(2)−Co(5)	57.34(4)
Co(2*)−Bi(2)−Co(3*)	53.23(5)	Co(4)−Bi(2)−Co(5)	57.05(4)
Co(2*)−Bi(2)−Co(4)	90.70(5)	Bi(1*)−Co(1)−Bi(2)	89.36(6)
Co(2*)−Bi(2)−Co(5)	56.80(4)	Bi(1*)−Co(1)−Co(2)	63.25(6)
Bi(1*)−Co(1)−Co(4)	121.67(8)	Bi(1*)−Co(2)−Bi(2*)	87.92(5)
Bi(1*)−Co(1)−Co(5)	60.42(4)	Bi(1*)−Co(2)−Co(1)	63.41(6)
Bi(1*)−Co(2)−Co(3)	122.90(7)	Bi(1)−Co(3)−Co(4)	62.92(6)
Bi(1*)−Co(2)−Co(5)	60.78(4)	Bi(1)−Co(3)−Co(5)	60.84(4)
Bi(2*)−Co(2)−Co(1)	123.28(7)	Bi(2*)−Co(2)−Co(3)	62.96(6)
Bi(2*)−Co(2)−Co(5)	60.85(4)	Bi(2*)−Co(3)−Co(2)	63.81(6)
Bi(2*)−Co(3)−Co(4)	122.55(7)	Bi(2*)−Co(3)−Co(5)	60.98(4)
Co(1)−Co(2)−Co(3)	91.81(8)	Co(1)−Co(2)−Co(5)	62.45(6)
Co(2)−Co(3)−Co(4)	88.61(7)	Co(2)−Co(3)−Co(5)	61.62(6)
Co(3)−Co(2)−Co(5)	62.15(6)	Co(4)−Co(3)−Co(5)	61.58(5)
Bi(1)−Co(3)−Bi(2*)	89.74(6)	Bi(1)−Co(4)−Bi(2)	88.72(5)
Bi(1)−Co(3)−Co(2)	122.43(7)	Bi(1)−Co(4)−Co(1)	123.28(8)
Bi(1)−Co(4)−Co(3)	63.20(6)	Bi(1)−Co(5)−Bi(1*)	180.00
Bi(1)−Co(4)−Co(5)	61.05(4)	Bi(1)−Co(5)−Bi(2)	89.46(3)
Bi(1)−Co(5)−Bi(2*)	90.54(3)	Bi(1)−Co(5)−Co(1)	118.06(4)
Bi(2)−Co(4)−Co(1)	62.95(6)	Bi(1)−Co(5)−Co(1*)	61.94(4)
Bi(2)−Co(4)−Co(3)	123.04(7)	Bi(1)−Co(5)−Co(2)	117.83(4)
Bi(2)−Co(4)−Co(5)	61.04(4)	Bi(1)−Co(5)−Co(2*)	62.17(4)
Co(1)−Co(4)−Co(3)	91.29(8)	Bi(1)−Co(5)−Co(3)	61.61(4)
Co(1)−Co(4)−Co(5)	62.24(6)	Bi(1)−Co(5)−Co(3*)	118.39(4)
Bi(1*)−Co(5)−Bi(2*)	89.46(3)	Bi(1)−Co(5)−Co(4)	61.57(4)
Bi(1*)−Co(5)−Co(1)	61.94(4)	Bi(1)−Co(5)−Co(4*)	118.43(4)
Co(3)−Co(4)−Co(5)	62.00(6)	Bi(1*)−Co(5)−Bi(2)	90.54(3)
Bi(1*)−Co(5)−Co(4*)	61.57(4)	Bi(1*)−Co(5)−Co(1*)	118.06(4)
Bi(2)−Co(5)−Bi(2*)	180.00	Bi(1*)−Co(5)−Co(2)	62.17(4)
Bi(2)−Co(5)−Co(1)	61.46(4)	Bi(1*)−Co(5)−Co(2*)	117.83(4)
Bi(1*)−Co(5)−Co(3)	118.39(4)	Bi(1*)−Co(5)−Co(3*)	61.61(4)
Bi(1*)−Co(5)−Co(4)	118.43(4)	Co(1*)−Co(5)−Co(4*)	56.50(5)
Bi(2)−Co(5)−Co(1*)	118.54(4)	Co(2)−Co(5)−Co(2*)	180.00
Bi(2)−Co(5)−Co(2)	117.65(4)	Co(2)−Co(5)−Co(3)	56.24(5)
Bi(2)−Co(5)−Co(2*)	62.35(4)	Co(2)−Co(5)−Co(3*)	123.76(5)
Bi(2)−Co(5)−Co(3)	118.32(4)	Co(2)−Co(5)−Co(4)	82.73(5)
Bi(2)−Co(5)−Co(3*)	61.68(4)	Co(2)−Co(5)−Co(4*)	97.27(5)
Bi(2)−Co(5)−Co(4)	61.90(4)	Co(2*)−Co(5)−Co(3)	123.76(5)
Bi(2)−Co(5)−Co(4*)	118.10(4)	Co(2*)−Co(5)−Co(3*)	56.24(5)
Bi(2*)−Co(5)−Co(1)	118.54(4)	Co(2*)−Co(5)−Co(4)	97.27(5)
Bi(2*)−Co(5)−Co(1*)	61.46(4)	Co(2*)−Co(5)−Co(4*)	82.73(5)
Bi(2*)−Co(5)−Co(2)	62.35(4)	Co(3)−Co(5)−Co(3*)	180.00
Bi(2*)−Co(5)−Co(2*)	117.65(4)	Co(3)−Co(5)−Co(4)	56.42(5)
Bi(2*)−Co(5)−Co(3)	61.68(4)	Co(3)−Co(5)−Co(4*)	123.58(5)
Bi(2*)−Co(5)−Co(3*)	118.32(4)	Co(3*)−Co(5)−Co(4)	123.58(5)
Bi(2*)−Co(5)−Co(4)	118.10(4)	Co(3*)−Co(5)−Co(4*)	56.42(5)
Bi(2*)−Co(5)−Co(4*)	61.90(4)	Co(4)−Co(5)−Co(4*)	180.00
Co(1)−Co(5)−Co(1*)	180.00	Co(1)−Co(5)−Co(4*)	123.50(5)
Co(1)−Co(5)−Co(2)	56.20(5)	Co(1*)−Co(5)−Co(2)	123.80(5)
Co(1)−Co(5)−Co(2*)	123.80(5)	Co(1*)−Co(5)−Co(2*)	56.20(5)
Co(1)−Co(5)−Co(3)	84.79(5)	Co(1*)−Co(5)−Co(3)	95.21(5)
Co(1)−Co(5)−Co(3*)	95.21(5)	Co(1*)−Co(5)−Co(3*)	84.79(5)
Co(1)−Co(5)−Co(4)	56.50(5)	Co(1*)−Co(5)−Co(4)	123.50(5)

[a] An asterisk denotes a distance or angle involving the symmetry-related equivalent atom.

previously described.[23] KC_8 is an effective reducing agent for carrying out this transformation, and the residual graphite is easily removed by filtration, giving a solution consisting of a mixture of $K[Bi_2Co_4(CO)_{11}]$ and $K[Co(CO)_4]$. Cation exchange with [PPN]Cl at this point allows separation of $[Bi_2Co_4(CO)_{11}]^-$ and $[Co(CO)_4]^-$, which have differing solubility properties as $[PPN]^+$ salts; however, when this procedure is performed, the reaction with $Mo(CO)_3$(toluene) proceeds so slowly that a significant degree of decomposition of the moderately stable cluster anion $[Bi_2Co_4(CO)_{11}]^-$ occurs, greatly lowering the product yield. It is desirable to have the product(s) of the reaction of the former compound with $Mo(CO)_3$(toluene) as a salt of the large, stabilizing counterion $[PPN]^+$. Therefore, the mixture of K^+ salts is used directly in order to achieve a more rapid reaction rate, and cation exchange is performed afterward, at which time the $[Co(CO)_4]^-$ anion may be separated along with the $Mo(CO)_6$ byproduct. The product as its K^+ salt is freely soluble in THF, MeCN, and MeOH and moderately soluble in Et_2O. The corresponding $[PPN]^+$ salt, however, is insoluble in Et_2O and MeOH, allowing it to be separated from the other compounds present in solution. This product dissolves rapidly in THF, giving a deep brown solution. In more polar solvents, such as MeCN, the compound decomposes over a period of several hours to give metallic residues. For this reason THF is the solvent of choice. Introduction of oxygen into the flask containing this solution at a rate sufficient to give the desired reaction is a difficult task. The rate must not be too fast so that only metal oxides are produced but must be fast enough to prevent loss of material caused by the instability of this reactant. This complicates attempts to selectively produce either $[PPN]_2[\mathbf{1}]$ or $[PPN]_2[\mathbf{2}]$. It is possible to produce $[PPN]_2[\mathbf{2}]$ as the only cluster product of the oxidation upon very slow introduction of oxygen; however, the production of $[PPN]_2[\mathbf{1}]$ requires a more rapid, albeit still slow, reaction. As a result, optimization of both the rate of formation and yield of $[PPN]_2[\mathbf{1}]$ is problematic. The synthesis of $[PPN]_2[\mathbf{1}]$ to date has always been accompanied by production comparable quantities of $[PPN]_2[\mathbf{2}]$. In addition to air and oxygen, other mild oxidizing agents have been tried, such as $[Cu(MeCN)_4]BF_4$, but without success. Stronger oxidants such as peroxides give instantaneous decomposition to metallic mirrors. Compounds $[PPN]_2[\mathbf{1}]$ and $[PPN]_2[\mathbf{2}]$ are insoluble in all common organic solvents and water. Even very polar coordinating solvents such as DMSO and DMF do not dissolve these materials to any measurable extent. The magnetic data indicate that $[PPN]_2[\mathbf{1}]$ is paramagnetic, in agreement with its odd electron count of 127 MVEs.

Structures of $[PPN]_2[\mathbf{1}]\cdot 2THF$ and $[PPN]_2[\mathbf{2}]\cdot 1.08THF$. Both molecules pack in centrosymmetric triclinic cells with crystallographically imposed inversion symmetry. For $[PPN]_2[\mathbf{1}]\cdot 2THF$ the molecule is situated such that Co(5) lies on a crystallographic inversion center (Figure 1), while in $[PPN]_2[\mathbf{2}]\cdot 1.08THF$ the inversion center lies at the center of the ring formed from Co(6), Co(7), and their symmetry-related counterparts. There is one crystallographically unique $[PPN]^+$ counterion in each unit cell giving cation-to-anion ratios of 2:1. In addition, there is solvent THF in the crystal lattice giving a total of two THF molecules per cluster formula unit for $[PPN]_2[\mathbf{1}]$, but for $[PPN]_2[\mathbf{2}]$ the lattice solvent was found to be present only at 54% occupancy; hence, the empirical formula is $[PPN]_2[\mathbf{2}]\cdot 1.08THF$. The latter compound would be formulated also as a bis(THF) solvate, $[PPN]_2[\mathbf{2}]\cdot 2THF$, if the solvent molecules retained in the lattice were present at full occupancy.

The anions of $[\mathbf{1}]^{2-}$ and $[\mathbf{2}]^{2-}$ are clearly structurally related, and both have approximate D_{4h} symmetry. We discuss their

Table 3. Selected Bond Distances (Å) and Angles (deg) for $[PPN]_2[\mathbf{2}]\cdot 1.08THF$[a]

A. Distances

Bi(1)−Co(1)	2.723(3)	Co(2)−Co(3)	2.492(5)	Bi(3)−Co(6)	2.709(4)	Co(5)−Co(6)	2.554(4)
Bi(1)−Co(2)	2.713(3)	Co(2)−Co(5)	2.667(4)	Bi(3)−Co(7*)	2.715(3)	Co(5)−Co(6*)	2.615(4)
Bi(1)−Co(5)	2.751(3)	Co(3)−Co(4)	2.493(4)	Bi(4)−Co(1)	2.709(3)	Co(5)−Co(7)	2.563(5)
Bi(1)−Co(6*)	2.716(3)	Co(3)−Co(5)	2.673(4)	Bi(4)−Co(4)	2.704(3)	Co(5)−Co(7*)	2.624(4)
Bi(1)−Co(7)	2.701(3)	Bi(2)−Co(2)	2.721(3)	Bi(4)−Co(5)	2.815(3)	Co(6)−Co(7)	2.622(5)
Bi(2)−Co(3)	2.725(3)	Bi(2)−Co(6*)	2.744(4)	Bi(4)−Co(6)	2.706(3)	Co(6)−Co(7*)	2.654(4)
Bi(2)−Co(5)	2.710(3)	Bi(2)−Co(7*)	2.724(3)	Bi(4)−Co(7)	2.696(3)	Co(1)−Co(4)	2.482(5)
Bi(3)−Co(3)	2.716(3)	Co(4)−Co(5)	2.633(4)	Co(1)−Co(2)	2.487(4)	Co(1)−Co(5)	2.621(4)
Bi(3)−Co(4)	2.732(3)	Bi(3)−Co(5)	2.740(3)				

B. Angles

Co(1)−Bi(1)−Co(2)	54.45(9)	Co(4)−Bi(3)−Co(7*)	115.0(1)	Bi(2)−Co(5)−Bi(4)	175.7(1)	Co(1)−Co(5)−Co(2)	56.1(1)
Co(1)−Bi(1)−Co(5)	57.21(9)	Co(5)−Bi(3)−Co(6)	55.89(9)	Bi(2)−Co(5)−Co(1)	116.9(1)	Co(1)−Co(5)−Co(3)	82.8(1)
Co(1)−Bi(1)−Co(6*)	114.3(1)	Co(5)−Bi(3)−Co(7*)	57.52(9)	Bi(2)−Co(5)−Co(2)	60.78(8)	Co(1)−Co(5)−Co(4)	56.4(1)
Co(1)−Bi(1)−Co(7)	85.51(9)	Co(6)−Bi(3)−Co(7*)	58.59(9)	Bi(2)−Co(5)−Co(3)	60.82(9)	Co(1)−Co(5)−Co(6)	119.9(1)
Co(2)−Bi(1)−Co(5)	58.44(9)	Co(1)−Bi(4)−Co(4)	54.6(1)	Bi(2)−Co(5)−Co(4)	116.9(1)	Co(1)−Co(5)−Co(6*)	121.6(2)
Co(2)−Bi(1)−Co(6*)	90.4(1)	Co(1)−Bi(4)−Co(5)	56.60(8)	Bi(2)−Co(5)−Co(6)	122.9(1)	Co(1)−Co(5)−Co(7)	90.5(1)
Co(2)−Bi(1)−Co(7)	114.3(1)	Co(1)−Bi(4)−Co(6)	111.60(9)	Bi(2)−Co(5)−Co(6*)	62.00(9)	Co(1)−Co(5)−Co(7*)	177.1(2)
Co(5)−Bi(1)−Co(6*)	57.14(9)	Co(1)−Bi(4)−Co(7)	85.88(9)	Bi(2)−Co(5)−Co(7)	123.6(1)	Co(2)−Co(5)−Co(3)	55.6(1)
Co(5)−Bi(1)−Co(7)	56.1(1)	Co(4)−Bi(4)−Co(5)	56.94(8)	Bi(2)−Co(5)−Co(7*)	61.38(9)	Co(2)−Co(5)−Co(4)	83.7(1)
Co(6*)−Bi(1)−Co(7)	58.66(9)	Co(4)−Bi(4)−Co(6)	85.9(1)	Bi(3)−Co(5)−Bi(4)	91.32(8)	Co(2)−Co(5)−Co(6)	174.3(1)
Co(2)−Bi(2)−Co(3)	54.47(9)	Co(4)−Bi(4)−Co(7)	112.26(9)	Bi(3)−Co(5)−Co(1)	117.4(1)	Co(2)−Co(5)−Co(6*)	93.7(1)
Co(2)−Bi(2)−Co(5)	58.83(8)	Co(5)−Bi(4)−Co(6)	55.05(8)	Bi(3)−Co(5)−Co(2)	115.8(1)	Co(2)−Co(5)−Co(7)	120.8(2)
Co(2)−Bi(2)−Co(6*)	89.7(1)	Co(5)−Bi(4)−Co(7)	55.38(9)	Bi(3)−Co(5)−Co(3)	60.2(1)	Co(2)−Co(5)−Co(7*)	122.1(1)
Co(2)−Bi(2)−Co(7*)	116.58(9)	Co(6)−Bi(4)−Co(7)	58.1(1)	Bi(3)−Co(5)−Co(4)	61.1(1)	Co(3)−Co(5)−Co(4)	56.0(1)
Co(3)−Bi(2)−Co(5)	58.92(9)	Bi(1)−Co(1)−Bi(4)	93.64(9)	Bi(3)−Co(5)−Co(6)	61.5(1)	Co(3)−Co(5)−Co(6)	121.3(2)
Co(3)−Bi(2)−Co(6*)	116.15(9)	Bi(1)−Co(1)−Co(2)	62.57(9)	Bi(3)−Co(5)−Co(6*)	120.8(1)	Co(3)−Co(5)−Co(6*)	122.7(1)
Co(3)−Bi(2)−Co(7*)	90.94(9)	Bi(1)−Co(1)−Co(4)	124.0(1)	Bi(3)−Co(5)−Co(7)	123.1(1)	Co(3)−Co(5)−Co(7)	173.3(1)
Co(5)−Bi(2)−Co(6*)	57.29(9)	Bi(1)−Co(1)−Co(5)	61.94(9)	Bi(3)−Co(5)−Co(7*)	60.8(1)	Co(3)−Co(5)−Co(7*)	94.3(1)
Co(5)−Bi(2)−Co(7*)	57.76(9)	Bi(4)−Co(1)−Co(2)	126.6(1)	Co(4)−Co(5)−Co(6)	90.6(1)	Bi(3)−Co(6)−Co(5)	62.7(1)
Co(6)−Bi(2*)−Co(7)	57.3(1)	Bi(4)−Co(1)−Co(4)	62.6(1)	Co(4)−Co(5)−Co(6*)	177.3(1)	Bi(3)−Co(6)−Co(5*)	119.0(1)
Co(3)−Bi(3)−Co(4)	54.47(9)	Bi(4)−Co(1)−Co(5)	63.73(9)	Co(4)−Co(5)−Co(7)	119.3(1)	Bi(3)−Co(6)−Co(7)	122.0(1)
Co(3)−Bi(3)−Co(5)	58.68(9)	Co(1)−Co(2)−Co(3)	89.4(1)	Co(4)−Co(5)−Co(7*)	121.9(2)	Bi(3)−Co(6)−Co(7*)	60.8(1)
Co(3)−Bi(3)−Co(6)	114.3(1)	Co(1)−Co(2)−Co(5)	61.0(1)	Co(6)−Co(5)−Co(6*)	92.0(1)	Bi(4)−Co(6)−Co(5)	64.6(1)
Co(3)−Bi(3)−Co(7*)	91.32(9)	Co(4)−Bi(3)−Co(6)	85.3(1)	Co(6)−Co(5)−Co(7)	61.6(1)	Bi(4)−Co(6)−Co(5*)	120.9(1)
Co(4)−Bi(3)−Co(5)	57.52(8)	Co(3)−Co(2)−Co(5)	62.3(1)	Co(6)−Co(5)−Co(7*)	61.6(1)	Bi(4)−Co(6)−Co(7)	60.8(1)
Co(2)−Co(1)−Co(4)	90.8(1)	Bi(2)−Co(3)−Bi(3)	88.48(9)	Co(6*)−Co(5)−Co(7)	61.7(1)	Bi(4)−Co(6)−Co(7*)	125.1(1)
Co(2)−Co(1)−Co(5)	62.9(1)	Bi(2)−Co(3)−Co(2)	62.68(9)	Co(6*)−Co(5)−Co(7*)	60.0(1)	Co(5)−Co(6)−Co(5*)	88.0(1)
Co(4)−Co(1)−Co(5)	62.1(1)	Bi(2)−Co(3)−Co(4)	121.4(1)	Co(7)−Co(5)−Co(7*)	92.4(1)	Co(5)−Co(6)−Co(7)	59.4(1)
Bi(1)−Co(2)−Bi(2)	89.97(9)	Bi(2)−Co(3)−Co(5)	60.26(9)	Bi(1)−Co(6*)−Bi(2)	89.41(9)	Co(5)−Co(6)−Co(7*)	60.5(1)
Bi(1)−Co(2)−Co(1)	63.0(1)	Bi(1)−Co(2)−Co(5)	61.5(1)	Bi(1)−Co(6*)−Bi(3*)	87.7(1)	Co(5)−Co(6*)−Co(7)	60.2(1)
Bi(1)−Co(2)−Co(3)	123.8(1)	Bi(2)−Co(2)−Co(3)	62.85(9)	Bi(1)−Co(6*)−Bi(4*)	174.4(1)	Co(5)−Co(6*)−Co(7*)	58.2(1)
Bi(2)−Co(2)−Co(1)	121.4(1)	Bi(3)−Co(3)−Co(2)	123.2(1)	Bi(1)−Co(6*)−Co(5*)	120.9(1)	Co(7)−Co(6)−Co(7*)	90.4(1)
Bi(2)−Co(2)−Co(5)	60.39(9)	Bi(4)−Co(4)−Co(1)	62.8(1)	Bi(1)−Co(6*)−Co(5)	62.10(9)	Bi(1)−Co(6*)−Co(7*)	122.2(1)
Bi(3)−Co(3)−Co(4)	63.11(9)	Bi(4)−Co(4)−Co(3)	126.4(1)	Bi(1)−Co(6*)−Co(7)	60.39(9)	Bi(1)−Co(7)−Bi(2*)	175.9(1)
Bi(3)−Co(3)−Co(5)	61.11(9)	Bi(4)−Co(4)−Co(5)	63.6(1)	Bi(2)−Co(6*)−Bi(3*)	176.7(1)	Bi(1)−Co(7)−Bi(3*)	87.91(9)
Co(2)−Co(3)−Co(4)	90.4(1)	Co(1)−Co(4)−Co(3)	89.5(1)	Bi(2)−Co(6*)−Bi(4*)	88.3(1)	Bi(1)−Co(7)−Bi(4)	94.4(1)
Co(2)−Co(3)−Co(5)	62.1(1)	Co(1)−Co(4)−Co(5)	61.6(1)	Bi(2)−Co(6*)−Co(5*)	120.3(1)	Bi(1)−Co(7)−Co(5)	62.9(1)
Co(4)−Co(3)−Co(5)	61.2(1)	Co(3)−Co(4)−Co(5)	62.8(1)	Bi(2)−Co(6*)−Co(5)	60.7(1)	Bi(1)−Co(7)−Co(5*)	118.8(1)
Bi(3)−Co(4)−Bi(4)	93.90(9)	Bi(1)−Co(5)−Bi(2)	89.39(8)	Bi(2)−Co(6*)−Co(7*)	61.0(1)	Bi(1)−Co(7)−Co(6)	121.9(1)
Bi(3)−Co(4)−Co(1)	122.9(1)	Bi(1)−Co(5)−Bi(3)	175.9(1)	Bi(2)−Co(6*)−Co(7)	118.9(1)	Co(6)−Co(7)−Co(6*)	89.6(1)
Bi(3)−Co(4)−Co(3)	62.4(1)	Bi(1)−Co(5)−Bi(4)	90.7(1)	Bi(3)−Co(6)−Bi(4)	94.4(1)	Co(5)−Co(7*)−Co(6*)	57.9(1)
Bi(3)−Co(4)−Co(5)	61.38(9)	Bi(1)−Co(5)−Co(1)	60.9(1)	Bi(2)−Co(7*)−Bi(3)	88.52(9)	Bi(1)−Co(7)−Co(6*)	60.95(9)
Bi(1)−Co(5)−Co(2)	60.07(9)	Bi(4)−Co(5)−Co(1)	59.67(9)	Bi(2)−Co(7*)−Co(6)	118.6(1)	Bi(2)−Co(7*)−Bi(4*)	88.97(9)
Bi(1)−Co(5)−Co(3)	115.7(1)	Bi(4)−Co(5)−Co(2)	115.7(1)	Bi(3)−Co(7*)−Co(5*)	120.7(1)	Bi(3)−Co(7*)−Bi(4*)	174.6(1)
Bi(1)−Co(5)−Co(4)	117.2(1)	Bi(4)−Co(5)−Co(3)	115.4(1)	Bi(3)−Co(7*)−Co(6*)	121.5(1)	Bi(3)−Co(7*)−Co(5)	61.71(9)
Bi(1)−Co(5)−Co(6)	122.6(1)	Bi(4)−Co(5)−Co(4)	59.41(9)	Bi(4)−Co(7)−Co(5*)	120.9(1)	Bi(3)−Co(7*)−Co(6)	60.60(9)
Bi(1)−Co(5)−Co(6*)	60.8(1)	Bi(4)−Co(5)−Co(6)	60.31(9)	Bi(4)−Co(7)−Co(6*)	124.8(1)	Bi(4)−Co(7)−Co(5)	64.7(1)
Bi(1)−Co(5)−Co(7)	61.0(1)	Bi(4)−Co(5)−Co(6*)	121.6(1)	Co(5)−Co(7)−Co(5*)	87.6(1)	Bi(4)−Co(7)−Co(6)	61.16(9)
Bi(1)−Co(5)−Co(7*)	120.8(1)	Bi(4)−Co(5)−Co(7)	59.96(9)	Co(5)−Co(7)−Co(6*)	60.1(1)	Co(5)−Co(7)−Co(6)	59.0(1)
Bi(2)−Co(5)−Bi(3)	88.3(1)	Bi(4)−Co(5)−Co(7*)	122.0(1)	Co(5)−Co(7*)−Co(6)	59.8(1)		

[a] An asterisk denotes a distance or angle involving the symmetry related equivalent atom.

analysis first on the basis of the transition metal arrays which are built of Co_8 tetragonal prisms (peripheral atoms, labeled Co_p) centered by an additional interstitial cobalt atom Co_i (**3** and **4**, respectively; Chart 1). There are no Co−Co bonds along the long edges of the tetragonal prism. Each of the rectangular faces is capped by bridging Bi atoms which are also bound to the interstitial cobalt atom. An open coordination site on the bismuth atoms located at 180° from the Bi−Co(5) vectors is expected to be the location of the bismuth lone pair, suggesting that the bismuth atoms are best considered as Bi^{3+}. The Bi and Co atoms can also be segregated into layer units comprised of the Co_4 squares and the Bi_4Co cross-shaped units (**5**, **6**). The four coplanar Co_p atoms are each eight-coordinate, being bonded to two bismuth atoms, three cobalt atoms, and three carbonyl ligands. The Bi_4-Co_i units are planar as required by the crystallographic inversion center upon which the interstitial cobalt atom sits in $[PPN]_2[\mathbf{1}]$.

The anion $[\mathbf{2}]^{2-}$ can be viewed as two Co_8 tetragonal prisms

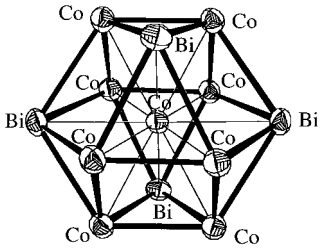

Figure 3. Alternative perspective of the anionic core of $[\mathbf{1}]^{2-}$ viewed down a pseudo-3-fold axis with the carbonyl ligands omitted for clarity.

as found in $[\mathbf{1}]^{2-}$ fused about one of the square faces. The atoms of the central, shared Co_4 square are designated as Co_c. As in $[\mathbf{1}]^{2-}$ a bismuth atom symmetrically caps each of the rectangular faces of both Co_8 tetragonal prisms. Additionally each bismuth atom is bonded to the interstitial Co_i atom (Co(5)). The Bi−Co_i distances on average are noticeably longer than the Bi−Co_p distances. The central Co_4 unit in $[PPN]_2[\mathbf{2}]$ is similar to the end Co_4 faces except that the μ-CO ligands are absent, resulting in ca. 0.15 Å longer Co−Co bond distances (2.623 Å, average). The Co_p−Co_i distances (average 2.62 Å) are somewhat longer than those within the Co_4 rings (2.47 Å, average), where the shortness of the distances is attributable to the presence of the μ-CO ligands. These values compare well to other CO-bridged Co−Co distances: 2.52(1)[32] and 2.550(2) Å[33] in $BiCo_3(CO)_9$ and 2.54(1)[34] or 2.538(3) Å[35] in $[Bi_2Co_4(CO)_{11}]^-$. The distances Co_p−Co_i in both anions are only slightly longer on average than Co_c−Co_i distances in $[\mathbf{2}]^{2-}$ ($[\mathbf{1}]^{2-}$, 2.615 Å; $[\mathbf{2}]^{2-}$, 2.649 Å vs 2.589 Å).

The interstitial cobalt atom Co(5) is 12-coordinate, a value associated with close-packing of metal spheres, suggesting that $[\mathbf{1}]^{2-}$ might be also viewed as a cuboctahedron. This is more clearly evident in Figure 3. In this view, the bismuth atoms are considered as vertexes of the metal cluster. The metal array can then be described as cubic close-packing (neglecting the difference in metal types). The cubic nature can be further noted in Figure 2 by considering the eight Bi atoms to lie at the corners of a hypothetical cubic unit cell. The Co atoms of the central square array and the interstitial cobalt atoms are seen to lie in the centers of the six faces of the Bi_8 cube.

Discussion

The product of the reaction between $K[Bi_2Co_4(CO)_{11}]$ and $Mo(CO)_3$(toluene) has a complex infrared spectrum and has not been isolated in pure form; however, the slow oxidation of this product in THF solution with adventitious air over several weeks has produced the novel new bismuth−cobalt carbonyl cluster $[\mathbf{2}]^{2-}$ in crystalline form. More rapid oxidation by brief exposure to air produces the related cluster $[\mathbf{1}]^{2-}$ as well as $[\mathbf{2}]^{2-}$. Both of these clusters are produced along with significant amounts of insoluble solids which lack CO stretching bands in the infrared spectrum. These clusters are insoluble in all common organic solvents and water. Compound $[\mathbf{1}]^{2-}$ is paramagnetic, with a magnetic moment of 2.24 μ_B consistent with a single unpaired electron as expected from the odd electron count.

Electronic Structure of the Anion $[\mathbf{1}]^{2-}$. Starting with a regular cube capped on four faces (**8**), the metal framework

Scheme 1

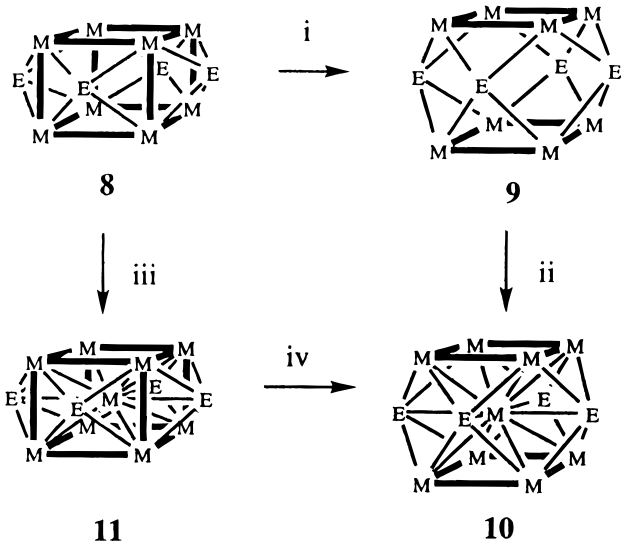

i. tetragonal distortion of empty tetracapped cube
ii. centering of tetragonally distorted tetracapped cube
iii. centering of empty tetracapped cube
iv. tetragonal distortion of centered tetracapped cube

found for $[\mathbf{1}]^{2-}$ can be generated in one of two ways (Scheme 1). One can first modify the structure by carrying out a tetragonal distortion to give **9** followed by insertion of the center metal atom (**10**) or the regular cube may be centered first (**11**) and then elongated. Being viewed as a metal-centered elongated tetracapped cubic (TCC) Co_8 cage, the cluster anion of $[\mathbf{1}]^{2-}$ bears a close structural and orbital resemblance to the HCC $M_9(\mu_4\text{-E})_6$ species.[12−17] For instance, the 124-MVE compound $Ni_9(\mu_4\text{-Bi})_6(PPh_3)_8$ reported by Fenske et al.[17] is similar to $[\mathbf{1}]^{2-}$ in terms of the core arrangement except for two major differences: (i) The Ni_9 cluster exhibits 12 Ni_p−Ni_p bonds and no direct Bi−Ni_i interactions while for $[\mathbf{1}]^{2-}$ there are only 8 Co_p−Co_p bonds with 4 additional Bi−Co_i bonds, and (ii) the centered Ni_9 cube is capped on all faces by bismuth atoms while $[\mathbf{1}]^{2-}$ has only four capped faces. These HCC $M_9(\mu_4\text{-E})_6L_8$ compounds, known only for M = Ni or Pd so far, have electron counts varying from 121 to 130,[18a] whereas their noncentered $M_8(\mu_4\text{-E})_6L_8$ parents possess a maximum of 120 MVEs.[18a] With 127 MVEs, cluster $[\mathbf{1}]^{2-}$ extends this class of compounds.

A previous analysis of the electronic structure of these various metallic cubic M_9E_6 clusters by some of us has shown that different electron counts are allowed depending on (i) the magnitude of the interaction of the d orbitals of the interstitial metal atom with its capped cubic cage and (ii) the nature of the capping E ligands (either bare or substituted).[18b] The weak Jahn−Teller unstability of such architectures with respect to the variation of MVE originates from the high connectivity of the centered HCC cage, a behavior reminiscent of solid-state structures.

To provide a comparison with these $M_9(\mu_4\text{-E})_6L_8$ cubic clusters and to understand the bonding in $[\mathbf{1}]^{2-}$, a detailed extended Hückel investigation, complemented with density functional theory calculations, has been carried out on this compound. The electronic structure can be described as resulting from the interaction between the interstitial Co atom and its $Co_8Bi_4(CO)_{16}$ host. The MO diagram of the $Co_8Bi_4(CO)_{16}$ cuboctahedral fragment itself is derived from that of a regular TCC cage (**8** in Scheme 1).[36] The EH MO diagram of the latter is shown on the left-hand side of Figure 5.

(32) Whitmire, K. H.; Leigh, J. S.; Gross, M. E. *J. Chem. Soc., Chem. Commun.* **1987**, 926.
(33) Martinengo, S.; Ciani, G. *J. Chem. Soc., Chem. Commun.* **1987**, 1589.
(34) Foust, A. S.; Dahl, L. F. *J. Am. Chem. Soc.* **1970**, *92*, 7337.
(35) Leigh, J. S.; Whitmire, K. H. *Angew. Chem., Int. Ed. Engl.* **1988**, *27*, 396.

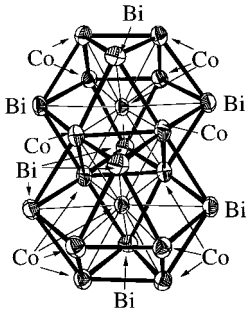

Figure 4. Alternative perspective of the anionic core of $[\mathbf{2}]^{2-}$ viewed down a pseudo-3-fold axis with the carbonyl ligands omitted for clarity.

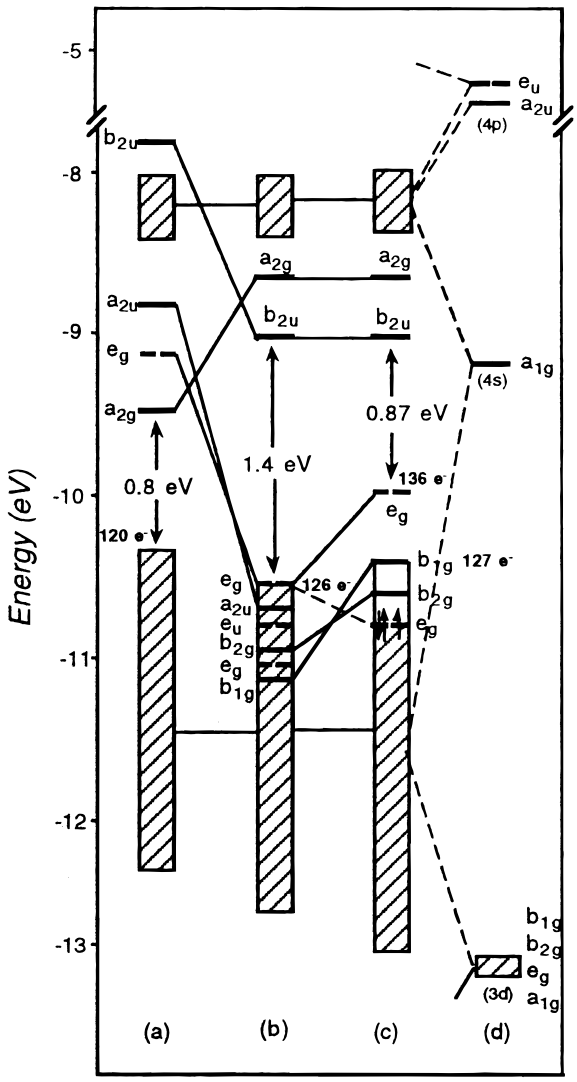

Figure 5. EHMO diagrams for (a) the 120-MVE tetracapped cubic model $[Co_8(\mu_4\text{-}Bi)_4(CO)_8(\mu\text{-}CO)_8]^{4-}$, (b) the hypothetical 126-MVE elongated cubic fragment $[Co_8(\mu_5\text{-}Bi)_4(CO)_8(\mu\text{-}CO)_8]^{10-}$, (c) the 127-MVE species $[\mathbf{1}]^{2-}$, and (d) the interstitial Co atom.

Although the symmetry of the TCC $Co_8(\mu_4\text{-}Bi)_4(CO)_8(\mu\text{-}CO)_8$ (**8**) unit is D_{4h}, its MO diagram strongly ressembles the general diagram[18a] of the O_h HCC $M_8(\mu_4\text{-}E)_6L_8$ clusters. In particular it shows a significant HOMO−LUMO gap for the count of 120 MVE, which corresponds to an electron-precise situation with 12 localized 2-electron M−M bonds associated with 18-electron metal centers. Indeed, in the transformation from HCC $M_8(\mu_4\text{-}E)_6L_8$ to TCC $M_8(\mu_4\text{-}E)_4L_8(\mu\text{-}CO)_8$, the formal substitution of two μ_4-E ligands by a set of eight bridging carbonyls does not change the pseudosymmetry of the occupied MOs. For the closed-shell MVE count of 120, both TCC and HCC cages are isolobal.

The TCC $(\mu_4\text{-}E)_4\{ML_n\}_8$ fragment **8** can be converted into an elongated TCC array **9** by stretching along the 4-fold axis (see Scheme 1). In principle, carrying this process out until four M−M localized bonds are broken is expected to result in the stabilization of four σ-antibonding levels (of b_{2u}, a_{2u}, and e_g symmetry), creating a HOMO−LUMO gap for MVE = 128. The energy level correlation diagram corresponding to the **8** → **9** distortion of $Co_8(\mu_4\text{-}Bi)_4(CO)_8(\mu\text{-}CO)_8$ is sketched in the left-hand side of Figure 5. It shows, however, that only the three levels of a_{2u} and e_g symmetry are significantly stabilized. The favored MVE count for a hypothetical cluster of type **9**, secured by a large HOMO−LUMO gap, would therefore be 126 and not 128 as expected.

There are two factors preventing the b_{2u} level from crossing the HOMO−LUMO gap upon elongation of the metallic cube. One is the fact that this level is the out-of-phase combination of two π Co−Co antibonding orbitals of the two Co_4 squares. Since the squares are preserved upon distortion, their π-antibonding character remains intact in structure **9**, maintaining the b_{2u} level at a somewhat high energy. This effect is related to the existence of two possible MVE counts (64 or 62) for the square M_4L_n compounds, depending on the accessibility of their π^*(M−M) level.[37,38] The second factor originates from the fact that the crucial a_{2u} and e_g levels present some Co−Bi bonding character. This bonding character increases upon distortion, contributing to the lowering of these levels. On the other hand, the b_{2u} orbital cannot mix by symmetry with the Bi orbitals and consequently, cannot provide additional stabilization upon elongation of the cube.

The major interactions between the elongated TCC $Co_8(\mu_4\text{-}Bi)_4(CO)_8(\mu\text{-}CO)_8$ fragment and Co_i leading to $[\mathbf{1}]^{2-}$ (see **10** in Scheme 1) are shown on the right-hand side of Figure 5. Strong interactions occur between the high-lying diffuse 4s (a_{1g}) and 4p (e_u and a_{2u}) AOs of Co_i and some counterparts of the elongated TCC host. Consequently, the out-of-phase combinations are strongly destabilized and cannot be populated (see Figure 5). The interactions involving the low-lying and more contracted 3d AOs of Co_i are much weaker. The z^2 (a_{1g}) AO is essentially nonbonding, while the other 3d(Co_i) orbitals interact weakly with MO counterparts of the cage, partly through the Co_i−Bi contacts, leading to some destabilization of levels of e_g, b_{2g}, and b_{1g} symmetry at the top of the d band (Figure 5).

The resulting MO diagram of $[\mathbf{1}]^{2-}$ suggests a favored closed-shell MVE count of 136 for elongated TCC clusters of type **10** (126 electrons coming from **9** plus 10 electrons in the five 3d orbitals on the interstitial metal atom). Such a closed-shell configuration may exist with the appropriate type of metal atoms and ligands. It would probably constitute the upper MVE limit for structure **10**. Values lower than 136 would correspond to the depopulation of the upper d-block MOs, which are Co_p−Co_i and Bi−Co_i antibonding, strengthening the bonding of Co_i with the Co_8Bi_4 fragment. This is what happens for compound $[\mathbf{1}]^{2-}$. With a count of 127 MVEs, EH calculations indicate the open-shell electron configuration $(e_g)^3$ with the unpaired

(36) (a) Johnston, R. L.; Mingos, D. M. P. *J. Organomet. Chem.* **1985**, *280*, 419. (b) Mingos, D. M. P.; Johnston, R. L. *Struct. Bond. (Berlin)* **1987**, *68*, 29.

(37) Mingos, D. M. P.; Wales, D. J. *Introduction to Cluster Chemistry*, Prentice-Hall: Englewood Cliffs, NJ, 1990.

(38) (a) Halet, J.-F.; Hoffmann, R.; Saillard, J.-Y. *Inorg. Chem.* **1985**, *24*, 1695. (b) Halet, J.-F. *Coord. Chem. Rev.* **1995**, *143*, 637.

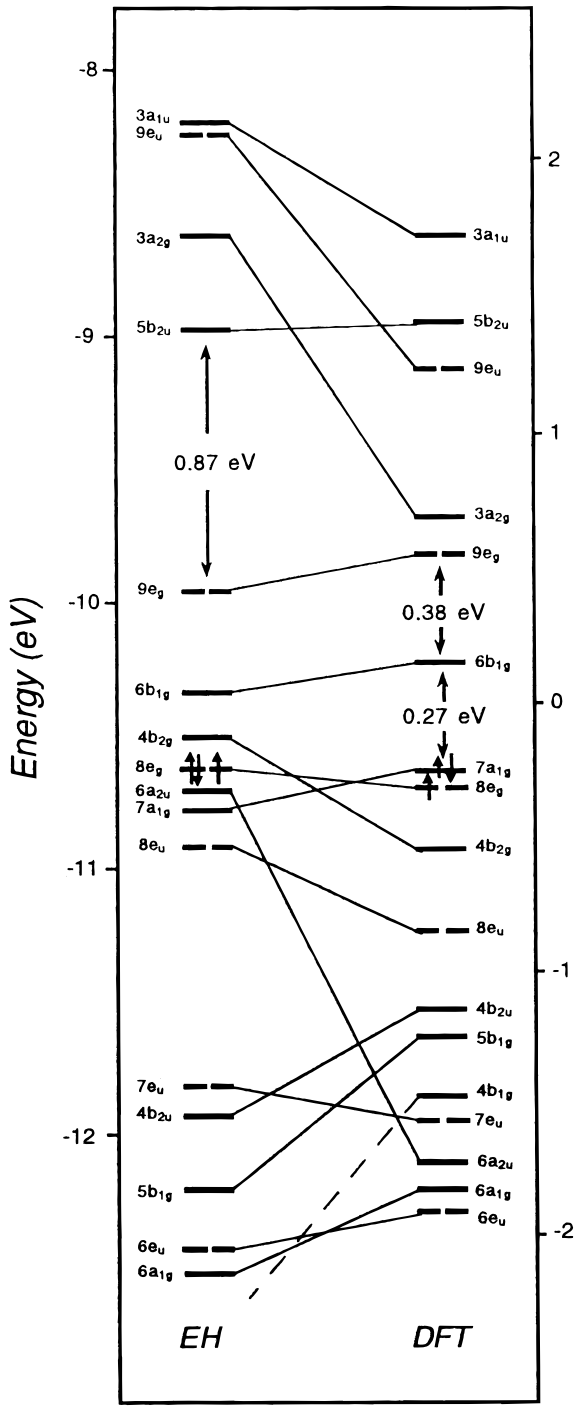

Figure 6. Comparison of the EH and DFT MO diagrams for $[\mathbf{1}]^{2-}$.

electron housed in an orbital lying just below the Co_p-Co_i and $Bi-Co_i$ antibonding b_{1g}, b_{2g}, and e_g MOs (see Figure 5). The EH Co_p-Co_p, Co_p-Bi, Co_p-Co_i, and Co_i-Bi overlap populations are 0.128, 0.248, 0.110, and 0.289, respectively. For a hypothetical MVE count of 136, they change to 0.108, 0.259, 0.048, and 0.218, respectively.

To get more reliable information concerning the open-shell configuration of compound $[\mathbf{1}]^{2-}$, DFT calculations were performed. For the sake of comparison, the EH and DFT MO diagrams are shown side by side in Figure 6. Their level orderings are in reasonable agreement, the major difference coming from some Bi-centered levels. The DFT electron configuration differs only slightly from that obtained with EH calculations: $[122](b_{2g})^2(e_g)^1(a_{1g})^2$ vs $[122](a_{1g})^2(e_g)^3(b_{2g})^0$, where [122] represents the unique configuration of the 122 lowest MVEs. A small HOMO−LUMO gap of 0.27 eV is found between $7a_{1g}$ and $6b_{1g}$. Other electron configurations were calculated such as $[122](b_{2g})^2(e_g)^2(a_{1g})^1$ and $[122](b_{2g})^2(e_g)^3(a_{1g})^0$. They were found less stable by 0.44 and 1.90 eV, respectively. The DFT atomic net charges for the ground-state are the following: −0.39 (Co_p), +0.81 (Bi), and +0.75 (Co_i). They compare well with the corresponding EH charges which are −0.27 (Co_p), +0.80 (Bi), and +0.64 (Co_i).

The electronic structure of $[\mathbf{1}]^{2-}$ differs somewhat from that of the metal-centered regular cubic species.[18a] An electronic structure comparable to that of $Ni_9(\mu_4\text{-}GeEt)_6(CO)_8$[18a] with a HOMO−LUMO gap of 1.26 eV for a count of 124 MVEs is computed for a regular cubic model $[\mathbf{1}]^+$ (**11** in Scheme 1). Stretching of the cube along the 4-fold axis leads to the stabilization of antibonding MOs which allows for larger electron counts.

An alternative way of describing cluster $[\mathbf{1}]^{2-}$ is to view it as a metal-centered four-connected cuboctahedral molecule with the capping Bi atoms considered as vertexes (see Figure 3). A noncentered 12-vertex *closo* arrangement of this type is generally characterized by 26 skeletal electrons, which corresponds to MVE = 122 for an M_8E_4 cluster.[36,37,39] This would lead to the favored closed-shell MVE count of 132 for an M_9E_4 metal-centered cuboctahedron, assuming no participation of the M_i d AO's to the bonding. Thus, from the vantage point of the hypothetical closed-shell MVE count of 136 for clusters of type **10** (see above), these compounds appear to be electron-rich with respect to the icosahedral derivation. In fact, this difference comes from the empty M_8E_4 cuboctahedral cage. As said above, our calculations on the D_{4h} $Co_8(\mu_4\text{-}Bi)_4(CO)_8(\mu\text{-}CO)_8$ framework of type **9** suggest a favored MVE count of 126 (vs 122 for a regular cuboctahedron). It turns out that the four extra electrons lie in an e_g level which, in the regular O_h cuboctahedron, is part of the degenerate t_{1g} LUMO. The main reason for the low energy of this e_g level (actually the HOMO) in **9** lies in the large electronegativity difference between Bi and Co which splits the t_{1g} level of the O_h framework considerably. Actually, the skeletal level ordering of $[\mathbf{1}]^{2-}$ is that of an elongated X_6 (X = E, M) cuboctahedron,[36] which is in fact a reasonable description of $[\mathbf{1}]^{2-}$.

Electronic Structure of $[\mathbf{2}]^{2-}$. As mentioned above, compound $[\mathbf{2}]^{2-}$ results from the condensation of two TCC clusters of type $[\mathbf{1}]^{2-}$ through one of their Co_4 square faces. A simplistic way of relating the electron counts of $[\mathbf{1}]^{2-}$ and $[\mathbf{2}]^{2-}$ would be to use the principle of *polyhedral fusion*,[40] assuming that the closed-shell favored count for $[\mathbf{1}]^{2-}$ is 128 (a value close to the actual count of 127). A simplistic application of this principle leads to the actual electron count of $[\mathbf{2}]^{2-}$ ($(128 \times 2) - 64 =$ 192 MVEs; 64 being one possible electron count of a square metal cluster[37]). However, it appears that this relationship is accidental since no significant HOMO−LUMO gap corresponding to MVE = 128 is computed for $[\mathbf{1}]^{2-}$ (see Figure 6) or for $[\mathbf{2}]^{2-}$ in the case of MVE = 192 (Figure 7, center, and Figure 8).

The EHMO electronic structure of $[\mathbf{2}]^{2-}$ can be derived from the interaction of the $(Co_i)_2$ fragment (right-hand side of Figure 7) with its $Co_{12}Bi_8(CO)_{12}(\mu\text{-}CO)_8$ host (left-hand side of Figure 7). It is noteworthy that a significant HOMO−LUMO gap, corresponding to an MVE count of 190, is found for the empty

(39) (a) Mingos, D. M. P.; Lin, Z. *J. Chem. Soc., Dalton Trans.* **1988**, 1657. (b) Mingos, D. M. P.; Lin, Z. *J. Organomet. Chem.* **1988**, *341*, 523.
(40) Mingos, D. M. P. *J. Chem. Soc., Chem. Commun.* **1983**, 706.

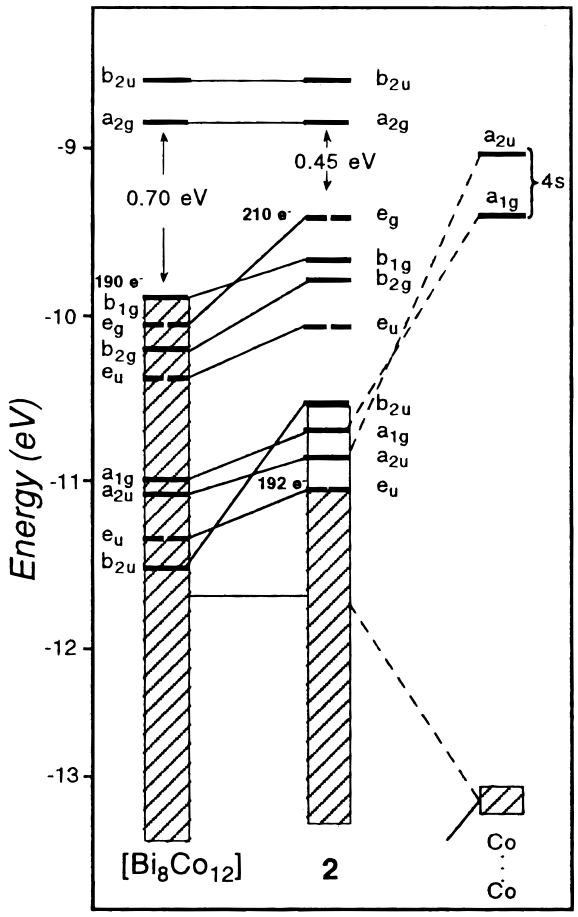

Figure 7. Interaction EH MO diagram for $[\mathbf{2}]^{2-}$.

fragment $Co_{12}Bi_8(CO)_{12}(\mu\text{-}CO)_8$. Such a hypothetical closed-shell electron count corresponds to that obtained from the condensation of two closed-shell 126-MVE M_8E_4 fragments sharing a square face ((126 × 2) − 62); 62 being an alternative electron count for a square metal cluster).[37]

When the Co_i atoms enter in their $Co_{12}Bi_8$ host, interactions comparable to that observed in compound $[\mathbf{1}]^{2-}$ occur. Here again, strong interactions are noted between the high-lying diffuse 4s and 4p combinations of the two Co_i atoms and some counterparts of the metallic cage. The low-lying d orbitals interact somewhat with the top of the d-block of the $Co_{12}Bi_8$ host, leading to a slight destabilization of the latter. A HOMO−LUMO gap of 0.45 eV would correspond to a complete filling of this band, i.e. to an MVE count of 190 + (2 × 10) = 210. However, as noted above for $[\mathbf{1}]^{2-}$, the depopulation of the upper MOs which are Co_i-Co_p, Co_i-Co_c, and Co_i-Bi antibonding enhances the stability of the cluster by strengthening the bonding between the interstitial Co atoms and the $Co_{12}Bi_8$ fragment. The EH Co_p-Co_p, Co_c-Co_c, Co_p-Bi, Co_c-Bi, Co_i-Co_p, Co_i-Co_c, and Co_i-Bi overlap populations are 0.109, 0.119, 0.261, 0.204, 0.099, 0.084, and 0.262 for the observed count of 192 electrons, respectively. For the hypothetical count of 210 MVEs, they change to 0.093, 0.172, 0.261, 0.224, 0.053, 0.055, and 0.219, respectively.

DFT calculations on the $(e_u)^4(a_{2u})^0$ singlet state of $[\mathbf{2}]^{2-}$ gave a very small HOMO−LUMO gap of 0.03 eV. This is consistent with a metal band-type electronic structure. The five lowest states were calculated to be very close in energy, lying within a range of 0.15 eV. Actually, all of them are high-spin states associated with different occupations of the four highest levels of a_{2u}, a_{1g}, e_u, and e_g symmetry. The ground-state EH and DFT MO diagrams are shown side by side in Figure 7. As in the case of $[\mathbf{1}]^{2-}$, they are in a fairly good qualitative agreement.

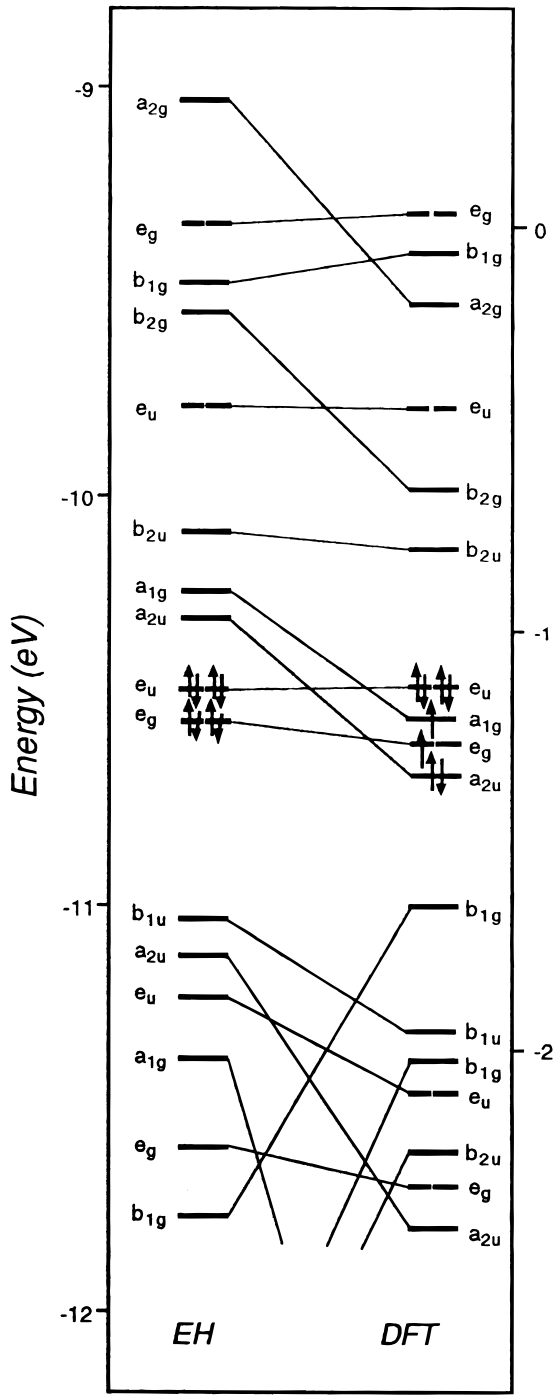

Figure 8. Comparison of the EH and DFT MO diagrams for $[\mathbf{2}]^{2-}$.

Related Structures and Compounds. Although the metal-centered Bi_4Co_9 cuboctahedron represents the most attractive geometric possibility for compound $[\mathbf{1}]^{2-}$, a metal-centered icosahedron (see **12** (Chart 2) for one possible isomer) may constitute an alternative arrangement. Mingos and Lin have shown that the (noncentered) icosahedral and cuboctahedral arrangements are expected to have identical electron counts (i.e. 122 MVEs for an M_8E_4 arrangement).[39] Few examples of noncentered or centered mixed transition metal−main group icosahedral species have been characterized.[41−48] As observed for the cubic compounds,[18] the noncentered and main-group-

(41) Vidal, J. L.; Troup, J. M. *J. Organomet. Chem.* **1981**, *213*, 351.

Chart 2

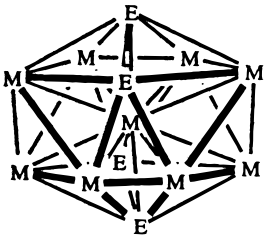

12

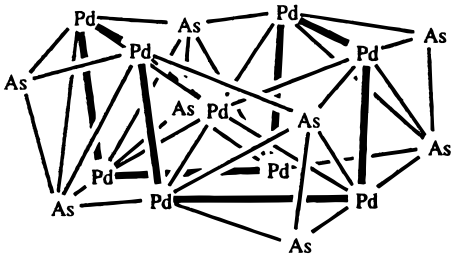

13

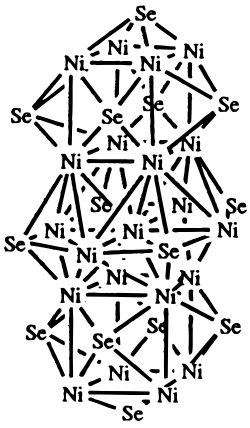

14

element-centered species follow the electron-counting rules better, while the metal-centered species are electron-rich.[48]

In addition to these discrete compounds, some solid-state phases have structural relationships to the ones considered here. In Ti_5Te_4 an infinite chain of face-sharing titanium-centered Ti_8 cubes are capped on the faces perpendicular to the chain by Te atoms in a similar arrangement to the buildup of layers shown as structure **6**.[49] The alternative icosahedral framework **12** appears in $BaCu_5Al_8$, which is composed of copper-centered $[Cu_4Al_8]^{2-}$ clusters.[50]

As said above, the metallic framework of $[\mathbf{1}]^{2-}$ can be viewed as resulting from the breaking of four M−M bonds along the edges of a regular centered cube. An alternative way of breaking four similar M−M bonds would result to the "D_{2d}" metallic arrangement observed in $Pd_9(\mu{:}\eta,{}^5\eta^2\text{-}As_2)_4(PPh_3)_8$[51] (**13**). Counting the $\mu{:}\eta,{}^5\eta^2$-As_2 ligands as 6-electron donor ligands, this cluster bears 130 MVEs, an electron count close to the one of $[\mathbf{1}]^{2-}$.

Condensation of octahedral transition metal−chalcogenide units sharing faces is largely exemplified in molecular and solid-state chemistry.[52] On the other hand, the condensation of cubic and/or cuboctahedric units is rather scarce so far. Anion $[\mathbf{2}]^{2-}$, which results from the condensation of two cuboctahedral fragments sharing a square face, is one example suggesting the posibility of larger clusters with additional Co_4 and Bi_4Co layers, leading ultimately to an infinite one-dimensional network. Our EH calculations on these hypothetical polymer and oligomers indicate that a full metallic situation (i.e. no significant HOMO−LUMO gap for any realistic electron count) is reached as soon as more than two cuboctahedral M_8E_4 units are fused.

Another example based on the same condensation principle, namely the Chinese lantern-shaped $Ni_{21}Se_{14}(PEt_2Ph)_{12}$ (**14**), has been reported.[4] Its structure is made of a selenium-tetracapped metal-centered Ni_{13} cuboctahedron fused with two Ni_8 cubes along the 4-fold axis. Assuming a full participation of the 3d Ni_i AOs to the bonding, the *polyhedral fusion* principle[40] leads to a favored closed-shell MVE count of 286 ($170 + (120 \times 2) - (62 \times 2)$). This value is relatively close to the actual count of 290 MVEs. However, preliminary EH calculations on compound **14** suggest a "metallic state" with no significant gap in the HOMO/LUMO region, which is made of MOs which are slightly antibonding between Ni_i atom and its surrounding Ni_p atoms, as noted for $[\mathbf{1}]^{2-}$ and $[\mathbf{2}]^{2-}$.[53]

Concluding Remarks

The theoretical analysis of $[\mathbf{1}]^{2-}$ and $[\mathbf{2}]^{2-}$ indicates that the bonding of the interstitial metal atom with the metallic host somewhat differs from that found in their related metal-centered cubic species $M_9(\mu_4\text{-}E)_6L_8$, due to stretching along the 4-fold axis. The HOMO/LUMO region is slightly antibonding between the interstitial Co atoms and the surrounding Bi and Co_p atoms. Although no HOMO−LUMO gaps are observed, the actual electron counts for $[\mathbf{1}]^{2-}$ and $[\mathbf{2}]^{2-}$ seem the best compromise for having strong Co_p-Co_i and $Bi-Co_i$ bonding. This observation is consistent with reported electron counts for other cubic clusters which in general tend to have open-shell configurations while closed-shell configurations are less common and correspond generally to the maximum number of electrons predicted by the orbital structure.

Acknowledgment. The Centre National de la Recherche Scientifique (J.-Y.S. and J.-F.H.) and the National Science Foundation (K.H.W.) are gratefully acknowledged for financial support of this work as well as for the cooperative international travel grant which has greatly facilitated these studies. Funding from the Robert A. Welch Foundation (K.H.W.) also helped support this work. B.Z. (permanent address: Institut de Chimie, Université de Constantine, Route Aïn-el-Bey, Algeria) gratefully acknowledges financial support from the Ministère des Affaires

(42) Rieck, D. F.; Rae, A. D.; Dahl, L. F. *J. Chem. Soc., Chem. Commun.* **1993**, 585.
(43) Rieck, D. F.; Gavney, J. A., Jr.; Norman, R. L.; Hayashi, R. K.; Dahl, L. F. *J. Am. Chem. Soc.* **1992**, *114*, 10369.
(44) Rieck, D. F.; Montag, R. A.; McKechnie, T. S.; Dahl, L. F. *J. Am. Chem. Soc.* **1986**, *108*, 1330.
(45) DesEnfants, R. E., II; Gavney, J. A., Jr.; Hayashi, R. K.; Rae, A. D.; Dahl, L. F.; Bjarnason, A. *J. Organomet. Chem.* **1990**, *383*, 543.
(46) Albano, V. G.; Demartin, F.; Iapalucci, M. C.; Longoni, G.; Monari, M.; Zanello, P. *J. Chem. Soc., Dalton Trans.* **1992**, 497.
(47) Longoni, G. *Pure Appl. Chem.* **1990**, *62*, 1183.
(48) Albano, V. G.; Demartin, F.; Iapalucci, M. C.; Laschi, F.; Longoni, G.; Sironi, A.; Zanello, P. *J. Chem. Soc., Dalton Trans.* **1991**, 739.
(49) Grønvold, F.; Kjekhus, A.; Raaum, F. *Acta Crystallogr.* **1961**, *14*, 930.
(50) Nordell, K. J.; Miller, G. J. *Croat. Chem. Acta* **1995**, *68*, 825.
(51) Fenske, D.; Persau, C. *Z. Allg. Chem.* **1991**, *593*, 61.
(52) Fenske D.; Krautscheid, H.; Müller, M. *Angew. Chem., Int. Ed. Engl.* **1992**, *31*, 321.
(53) Zouchoune, B.; Halet, J.-F.; Saillard, J.-Y. Unpublished results.

Etrangères, MAE Grant No. 90 MDU 136. F.O. is grateful to the Ministère de l′Education Nationale for a predoctoral grant. F.O., J.-F.H., and J.-Y. S. thank Pr. Baerends and Dr. te Velde (Vrije Universiteit, Amsterdam) for introducing them to the ADF program. Exchanges with Baerends' group have been made possible through an European Human Capital and Mobility Network Grant (ERBCHRXCT-930156). J.-F. H. and J.-Y. S. thank the Centre de Ressources Informatiques (CRI) of Rennes, France, and the Institut de Développement et de Ressources en Informatique Scientifique (IDRIS-CNRS) of Orsay, France, for computing facilities.

Supporting Information Available: Tables of data collection and refinement parameters, atomic coordinates and thermal parameters including hydrogens, complete bond distances and angles, and anisotropic displacement parameters (37 pages). Ordering information is given on any current masthead page.

IC970715B